Microcapsules

DOI: 10.1002/anie.201106723

Controlled Origami Folding of Hydrogel Bilayers with Sustained Reversibility for Robust Microcarriers**

*Tae Soup Shim, Shin-Hyun Kim, Chul-Joon Heo, Hwan Chul Jeon, and Seung-Man Yang**

Microencapsulation and controlled release have long been studied because of the high demand for practical delivery systems in the pharmaceutics and cosmetics fields. Multiphase emulsion drops have provided efficient templates for microcapsules, and various feasible methods have been developed for controlled release.[1] However, the emulsion-based approach has limitations for the in situ control of membrane permeability. Micro-origami has emerged as one of the most promising alternative approaches for producing tunable microcapsules with the potential to be applied, for example as drug carriers,[2] actuators,[3] microcontainers,[4] and microrobots.[5] Inspired by living organisms in nature such as the ice plant[6] and Venus flytrap,[7] two different micro-origami approaches have been employed to make various microstructures.[8] One approach uses solid patches connected by active hinge materials. Typical examples use various metal–metal,[9] metal–polymer,[10] and polymer–polymer[4] combinations. The patch and hinge system has enabled the capture, release, and gripping[11] of target materials, showing the feasibility of micro-origami structures. However, the microcapsule is limited to polyhedral shapes in this approach, and complete sealing of the gaps between patches requires exquisite control of the folding angles. Moreover, the delicate and complex fabrication processes make practical applications difficult. The second approach uses a bilayer structure composed of two different materials. For example, a metal–polymer bilayer can show bending/unbending when the polymeric active layer suffers significant volume change, but the metal layer remains unchanged.[12,13] Polymer materials have been employed in both layers to make biocompatible microcapsules.[14,15] However, complete sealing of the gaps in the bilayer contact regions remains an important, yet unmet, need. In addition, a simple and effective method for the fabrication of practical microcapsules has not yet been developed, and remains highly desirable. This is the main thrust of the present study.

[*] T. S. Shim, Dr. S.-H. Kim, Dr. C.-J. Heo, H. C. Jeon, Prof. S.-M. Yang
National Creative Research Initiative Center for Integrated Optofluidic Systems and
Department of Chemical and Biomolecular Engineering KAIST
Daejeon, 305-701 (Korea)
E-mail: smyang@kaist.ac.kr
Homepage: http://msfl.kaist.ac.kr

[**] This work was supported by a grant from the Creative Research Initiative Program of the Ministry of Education, Science, and Technology for "Complementary Hybridization of Optical and Fluidic Devices for Integrated Optofluidic Systems."

Supporting information for this article is available on the WWW under http://dx.doi.org/10.1002/anie.201106723.

Herein, we report the use of biocompatible bilayer structures for the fabrication of tunable microcapsules based on micro-origami. Monodisperse bilayer microstructures were prepared using a facile photolithographic procedure, without employing photomask alignment. In addition, highly flexible hydrogels were selected as both active and passive layers, facilitating tight contact between patches. The bilayer structure therefore enabled in situ encapsulation, through a reversible transformation to microcapsules with a closed compartment. The resultant microcapsules showed negligible leakage of encapsulants and triggered release of the encapsulants could be achieved simply by inducing the unfolding of the hydrogel bilayer.

The essential strategy of our approach relies on the anisotropic volume change of a hydrogel bilayer. As shown in Scheme 1 a, the active hydrogel layer shows significant volume expansion under external stimuli by swelling, whereas the passive hydrogel layer remains in a constant volume. Therefore, mechanical stress drives the bending of the bilayer, resulting in microcapsules with a closed compartment. The hydrogel swelling behavior is highly reversible, enabling repeated transformations.

The hydrogel bilayer structure was prepared on a glass substrate, using photolithography with an amorphous silicon photomask, as shown in Scheme 1 b. Here, we propose poly(2-hydroxyethyl methacrylate-*co*-acrylic acid), p(HEMA-*co*-AA), and poly(2-hydroxyethyl methacrylate), p(HEMA), as model components because they are widely used, FDA-approved (FDA = Food and Drug Administration) biocompatible materials. One monomer solution for p(HEMA-*co*-AA) was infiltrated into the space between the photomask and a polydimethylsiloxane (PDMS) microchannel of 25 μm thickness; this monomer solution was then polymerized by UV irradiation through the photomask. The second monomer solution for p(HEMA) was infiltrated into the space between the same photomask and a PDMS microchannel 50 μm in thickness, after washing out the previously unpolymerized solution. Upon the second round of UV irradiation, bilayer structures consisting of a p(HEMA) layer on a p(HEMA-*co*-AA) layer were formed; alignment of the photomask was unnecessary, because each layer was fabricated on the photomask. The resultant bilayer structures were released from the photomask through immersion in a pH 9 buffer solution.

To exploit the structural transformation of the bilayer microparticles, we used two different shapes of microparticle: snowman-shaped and flower-shaped. The shape and dimensions of these microparticles were carefully determined to ensure a fully closed compartment in the swollen state; both the snowman- and flower-shaped microparticles were 50 μm

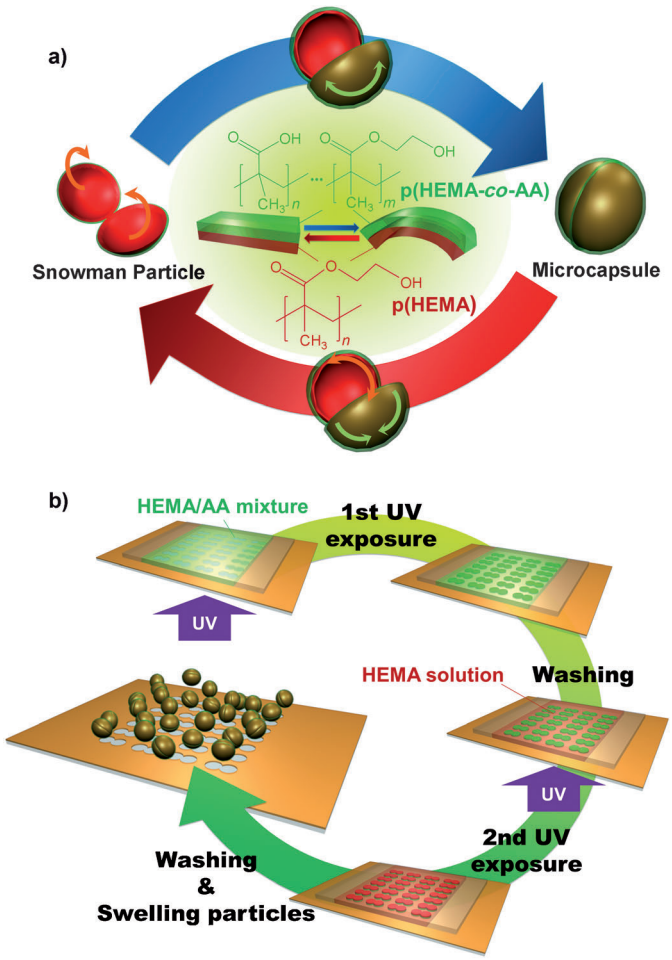

Scheme 1. a) Reversible structural transformation of a hydrogel bilayer, one consisting of p(HEMA-*co*-AA) and the second consisting of p(HEMA), depending on pH. b) Fabrication procedures of hydrogel bilayer microparticles based on photolithography.

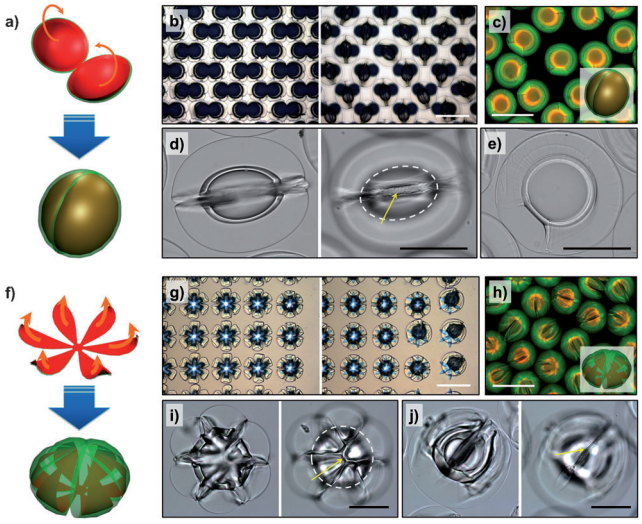

Figure 1. a) Transformation of snowman-shaped microparticles to a microcapsule. b) Optical microscope images of arrays of bilayer microparticles on a photomask and transformed microcapsules at pH 9. c) Confocal microscope image of microcapsules, inner layer consisting of R6G-tagged p(HEMA) and outer layer consisting of FITC-tagged p(HEMA-*co*-AA). d) Magnified optical microscope images of microcapsules in top view at two different focal planes and e) side view. f–j) A set of a scheme and optical and confocal microscope images of flower-shaped microparticles. Scale bars indicate 500 μm for b, c, g, and h, and 200 μm for d, e, i, and j, respectively.

in thickness (with 25 μm in each layer), and 400 μm in the largest lateral dimension. This aspect ratio of 1:8 is small enough to give a sufficient cavity volume, and large enough to achieve a high mechanical strength in the microcapsule structure. We used p(HEMA-*co*-AA) as an active material. This material is capable of swelling up to about 1000 v/v % under basic conditions.[16] Both the snowman- and flower-shaped microparticles (these shapes were presented on the photomask substrate) transformed into microcapsules when they were dispersed in a pH 9 buffer solution, as shown in Figure 1 b and g, respectively (see Movie S1 in the Supporting Information for the transformation of the snowman-shaped microparticles). Because p(HEMA-*co*-AA) swelled at high pH whereas p(HEMA) retained its structure, the planar bilayer particles folded, forming closed compartment. The structure and shape of the microcapsules were also confirmed using confocal microscopy (Figure 1 c and h). A p(HEMA-*co*-AA) layer was tagged with fluorescein isothiocyanate (FITC), and a p(HEMA) layer was tagged with rhodamine 6G (R6G). The swelling of the p(HEMA-*co*-AA) layer drove the folding of the bilayer, forming a closed outer layer of the microcapsules, whereas the p(HEMA) layer at constant volume bent to form the inner layer in both microparticles, as shown in Figure S1 in the Supporting Information. In magnified optical microscopy images of these microcapsules, we confirmed tight contact between the neighboring patches, as denoted with arrows in Figure 1 d, i, and j. The snowman-shaped microparticles formed oblate spheroids with a cavity inside. The two planar circles produce a cavity as they are superimposed; this is difficult to achieve with rigid materials. Because of the high flexibility of hydrogels, a planar circular bilayer can form a bowl through 2D bending. This result shows the great potential of soft materials as micro-origami structures; the passive layer remains in a constant volume, and simultaneously lowers the degree of swelling of the active layer at the boundary by limiting water transport through the passive layer, increasing the anisotropic swelling of the microparticle. The passive layer is therefore not just "a supporter", but "an enhancer" of the folding/unfolding behaviors. The flower-shaped microparticles formed spherical capsules. The white circles in the top-view (Figure 1 i) and side-view (Figure 1 j) images of the microcapsules show a spherical cavity closed by tight contact between the neighboring petals. The six petals swelled in both the lateral and longitudinal directions; lateral swelling enabled contact between the sides of each petal, and longitudinal swelling enabled contact to be made at the top between the six petals, without any holes.

The microparticle and capsule structures depend on the pH conditions in the dispersion medium. Monodisperse snowman-shaped microparticles are shown under three different pH conditions (pH 9, 7, and 4) in Figure 2 a–c, respectively. Under basic conditions, at pH 9, p(HEMA-*co*-

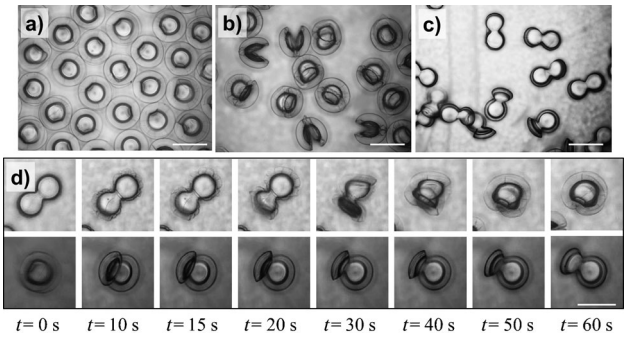

Figure 2. a–c) Optical microscope images of snowman-shaped microparticles dispersed in aqueous medium at a) pH 9, b) pH 7, and c) pH 4. d) Series of still-shot images showing a folding of a bilayer for sudden change of pH from 4 to 9 (upper row)and an unfolding of a bilayer (lower row); images are taken at denoted times from the first image. All scale bars indicate 400 μm.

AA) was highly swollen, and all microparticles formed a closed compartment at equilibrium. Under neutral conditions, at pH 7, the degree of swelling decreased, and the microparticle compartments were opened. Under acidic conditions, at pH 4, p(HEMA-*co*-AA) recovered its initial volume, and the microparticles showed a planar snowman-shaped configuration (see Figure S2 in the Supporting Information for the same set of flower-shaped microparticles). These results show that the bilayer structures can be dynamically tuned using the pH conditions. As shown in the top row of Figure 2d, when the pH of the dispersion medium was changed from 4 to 9, the snowman-shaped microparticle transformed into a microcapsule within 1 min. Under the reverse transition from pH 9 to 4, the microcapsule opened in 10 seconds, and unfolded into a planar snowman-shaped microparticle in 1 min (see Movie S2 in the Supporting Information). These folding and unfolding behaviors were highly reversible, and could be repeated without damaging the microparticle.

To show the in situ encapsulation and triggered release of target materials, we dispersed snowman-shaped microparticles in a suspension of 1 μm polystyrene particles at pH 9. The microparticles slowly folded and formed microcapsules with a closed compartment containing the particles, as shown in Figure 3a. The particles in the microcapsule cavity showed Brownian motion (as shown in Movie S3 in the Supporting Information), and could not escape from the cavity as long as the capsules were held under basic conditions. After the removal of unencapsulated particles by repeated washing with a buffer solution of pH 9, the microcapsules were redispersed into a buffer solution of pH 4. As soon as the capsules were dispersed, they began to open and allow the release of the particles, as shown in Figure 3c (see Movie S3 in the Supporting Information). Finally, all particles escaped from the unfolded microparticles, as shown in Figure 3b. To evaluate the permeability of the folded capsules, we also employed FITC–dextran molecules with two different molecular weights (of 10 K and 2000 K) as model encapsulants. In the same manner as the 1 μm particles, the FITC–dextran molecules were encapsulated at pH 9 and released at pH 4, as shown in Figure 3d. As the capsules opened, the dextran

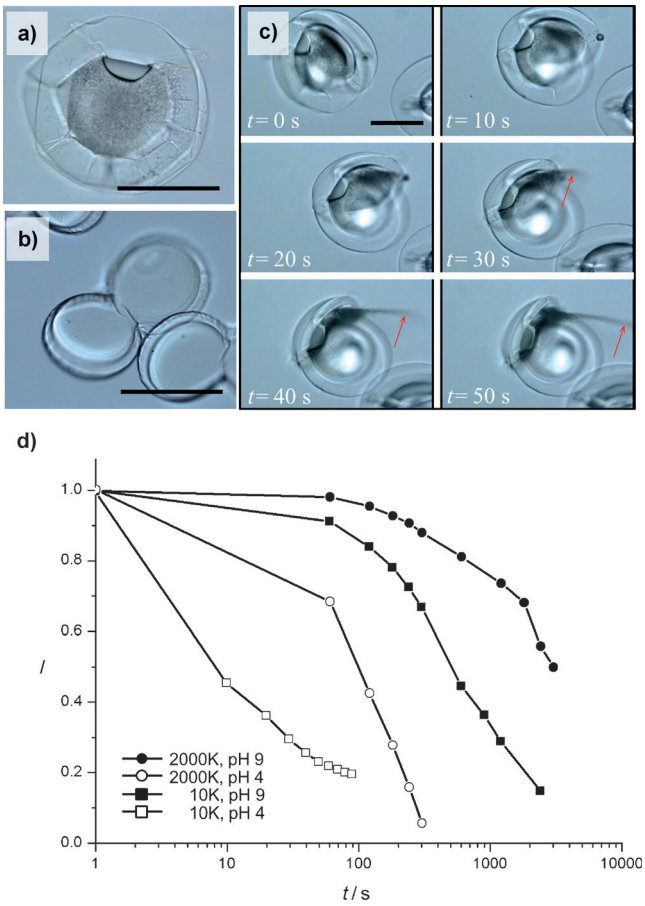

Figure 3. a,b) Optical microscope images of a) a microcapsule containing 1 μm particles and b) unfolded microparticle after release of the particles. c) Series of still images showing release of 1 μm particles upon sudden change of pH from 9 to 4. d) Fluorescence intensity of FITC–dextran molecules (*I*; molecular weights of 10 K and 2000 K) captured in a cavity of microparticles as a function of time; filled circles and squares denote the capsules at pH 9 and unfilled circles and squares denote the capsules which suffer sudden change of pH from 9 to 4 at $t = 0$ for 2000 K and 10 K molecules, respectively. All scale bars indicate 200 μm.

molecules were quickly diffused out. Half of the 10 K-dextran molecules were released within 10 seconds (unfilled squares), and half of the 2000 K-dextran molecules were released within 100 seconds (unfilled circles). When the capsules were dispersed in a buffer solution of pH 9, the release of the dextran molecules was remarkably retarded; it took over 500 seconds for half of the 10 K-dextran molecules (filled squares) to be released, and over 3000 seconds for half of the 2000 K-dextran molecules (filled circles) to be released, as shown in Figure 3d. We attribute this slow release of the molecules at pH 9 to nanoscale pores in the swollen hydrogel, and microscopic gaps between pairs of facing patches.

Magnetic functionality in the microparticles was achieved simply by adding iron(III) oxide nanoparticles to the monomer solution of the passive layer prior to photopolymerization. To induce a net magnetic moment, an external magnetic field was applied during polymerization which enabled the alignment of weakly ferromagnetic iron oxide nanoparticles in the hydrogel matrix.[17] The resultant magnetoresponsive

microcapsules could be concentrated using a magnetic field, as shown in Figure S3a in the Supporting Information. In addition, the net magnetic moment in the microparticles enabled rotation-induced locomotion on the substrate to occur under a rotating magnetic field, as shown in Figure S3b in the Supporting Information.

Herein, we have reported tunable microcapsules using a hydrogel bilayer structure, consisting of active and passive layers. The lithographically featured planar bilayer microparticles showed a structural transformation to microcapsules with a closed compartment, because of an anisotropic volume expansion in the hydrogel bilayer. This transformation between the planar microparticle and the microcapsule was highly reversible, and this bilayer structure was therefore useful for the in situ encapsulation and the triggered release of active ingredients, as shown here. The soft hydrogel materials enabled the formation of curved surfaces and tight contact between patches, facilitating the complete closure of compartments in the resultant microcapsules. This is difficult to achieve with previous approaches based on rigid materials. This novel hydrogel bilayer-based approach for the fabrication of tunable microcapsules is therefore promising for a wide range of applications such as drug delivery, cell encapsulation, tissue engineering scaffolds, and soft robotics, owing to the high reversibility of its actuation, the biocompatibility of materials, and the simplicity of fabrication.

Experimental Section

Preparation of hydrogel monomer solutions: We prepared two different hydrogel monomer solutions for a passive layer of p(HEMA) and a active layer of p(HEMA-*co*-AA). For p(HEMA), 1 wt% ethylene glycol dimethacrylate (EGDMA, Aldrich) and 3 wt% photoinitiator (Darocur 1173, Ciba Specialty Chemicals) were dissolved in 2-hydroxylethyl methacrylate (HEMA, Aldrich). For p(HEMA-*co*-AA), acrylic acid (AA, Aldrich) was added into the monomer solution for p(HEMA) in a molar ratio of 1:5. In addition, rhodamine 6G (R6G,Aldrich) and fluorescein isothiocyanate (FITC, TCI) were added to the monomer solutions for p(HEMA) and p(HEMA-*co*-AA) in a concentration of 4 mM, respectively. To make magnetoresponsive bilayer microparticles, 0.1 wt% iron(III) oxide nanoparticles (< 50 nm, hematite, Aldrich) were dispersed in HEMA solution.

Fabrication of bilayered hydrogel microparticles: To make amorphous silicon photomask, a photoresist (AZ5124, AZ Electronic Materials) was patterned on the amorphous silicon (a-Si) coated glass by conventional photolithography. Subsequently, a-Si was selectively removed by reactive ion etching with SF_6 (VSRIE-400A, Vacuum Science) and the photoresist was removed by acetone. For the active layer, the monomer solution for p(HEMA-*co*-AA) was infiltrated between the photomask and polydimethylsiloxane (PDMS) microchannel with 25 μm in thickness. After the first UV exposure, p(HEMA-*co*-AA) particles were washed by ethanol. For the passive layer, the monomer solution for p(HEMA) was infiltrated between the photomask and PDMS microchannel with 50 μm in thickness. Subsequently, the second UV exposure and washing step leaved bilayer microparticles on the photomask. For magnetoresponsive microparticles, a HEMA solution containing 0.1 wt% iron oxide nanoparticles was used for the passive layer, where UV exposure was conducted under a magnetic field to align the iron oxide nanoparticles.[17] To release the resultant microparticles, the photomask was immersed in buffer solution of pH 9.

Received: September 22, 2011
Published online: November 21, 2011

Keywords: encapsulation · hydrogels · origami structures · polymers

[1] a) I. G. Loscertales, A. Barrero, I. Guerrero, R. Cortijo, M. Marquez, A. M. Ganan-Calvo, *Science* **2002**, *295*, 1695 – 1698; b) A. S. Utada, E. Lorenceau, D. R. Link, P. D. Kaplan, H. A. Stone, D. A. Weitz, *Science* **2005**, *308*, 537 – 541; c) S.-H. Kim, H. Hwang, C. H. Lim, J. W. Shim, S.-M. Yang, *Adv. Funct. Mater.* **2011**, *21*, 1608 – 1615.

[2] H. Y. He, J. J. Guan, J. L. Lee, *J. Controlled Release* **2006**, *110*, 339 – 346.

[3] J. M. Z. Ocampo, P. O. Vaccaro, K. Kubota, T. Fleischmann, T.-S. Wang, T. Aida, T. Ohnishi, A. Sugimura, R. Izumoto, M. Hosoda, S. Nashima, *Microelectron. Eng.* **2004**, *73*, 429 – 434.

[4] A. Azam, K. E. Laflin, M. Jamal, R. Fernandes, D. H. Gracias, *Biomed. Microdevices* **2011**, *13*, 51 – 58.

[5] E. W. H. Jager, O. Inganas, I. Lundstrom, *Science* **2000**, *288*, 2335 – 2338.

[6] M. J. Harrington, K. Razghandi, F. Ditsch, L. Guiducci, M. Rueggeberg, J. W. Dunlop, P. Fratzl, C. Neinhuis, I. Burgert, *Nat. Commun.* **2011**, *2*, 337.

[7] Y. Forterre, J. M. Skotheim, J. Dumais, L. Mahadevan, *Nature* **2005**, *433*, 421 – 425.

[8] a) T. G. Leong, A. M. Zarafshar, D. H. Gracias, *Small* **2010**, *6*, 792 – 806; b) L. Ionov, *Soft Matter* **2011**, *7*, 6786 – 6791.

[9] T. Leong, Z. Y. Gu, T. Koh, D. H. Gracias, *J. Am. Chem. Soc.* **2006**, *128*, 11336 – 11337.

[10] T. G. Leong, B. R. Benson, E. K. Call, D. H. Gracias, *Small* **2008**, *4*, 1605 – 1609.

[11] J. S. Randhawa, M. D. Keung, P. Tyagi, D. H. Gracias, *Adv. Mater.* **2010**, *22*, 407 – 410.

[12] Y. Ma, J. Q. Sun, *Chem. Mater.* **2009**, *21*, 898 – 902.

[13] T. S. Kelby, M. Wang, W. T. S. Huck, *Adv. Funct. Mater.* **2011**, *21*, 652 – 657.

[14] G. Stoychev, N. Puretskiy, L. Ionov, *Soft Matter* **2011**, *7*, 3277 – 3279.

[15] N. Bassik, B. T. Abebe, K. E. Laflin, D. H. Gracias, *Polymer* **2010**, *51*, 6093 – 6098.

[16] L. Brannonpeppas, N. A. Peppas, *Biomaterials* **1990**, *11*, 635 – 644.

[17] S. H. Kim, J. Y. Sim, J. M. Lim, S. M. Yang, *Angew. Chem.* **2010**, *122*, 3874 – 3878; *Angew. Chem. Int. Ed.* **2010**, *49*, 3786 – 3790.

